

# Exciton decay dynamics controlled by impurity occupation in strongly Mn-doped and partially compensated bulk GaAs

F. Münzhuber, T. Henn, T. Kiessling,<sup>\*</sup> W. Ossau, and L. W. Molenkamp<sup>†</sup>*Physikalisches Institut Universität Würzburg, Lehrstuhl für Experimentelle Physik III, Am Hubland, 97074 Würzburg, Germany*B. Giesecking, G. V. Astakhov, and V. Dyakonov<sup>‡</sup>*Physikalisches Institut Universität Würzburg, Lehrstuhl für Experimentelle Physik VI, Am Hubland, 97074 Würzburg, Germany*

(Received 21 March 2014; revised manuscript received 4 September 2014; published 26 September 2014)

We report on a pronounced prolongation of the exciton decay in strongly *p*-doped and partially compensated direct band-gap semiconductor GaAs:Mn with increasing optical excitation power. Using time-resolved photoluminescence we show that the intricate interplay of excitons, shallow and deep impurity centers in GaAs:Mn results in a complex recombination behavior that cannot be characterized in terms of simple rates. The decay can be precisely described by a model based on Shockley-Read-Hall recombination, which shows that the observed dynamics arise from a varying neutralization of shallow and deep recombination centers. This enables the investigation of the carrier dynamics in the impurity system by measuring only the exciton decay time.

DOI: [10.1103/PhysRevB.90.125203](https://doi.org/10.1103/PhysRevB.90.125203)

PACS number(s): 71.55.Eq, 72.20.Jv, 78.47.D-, 85.75.-d

## I. INTRODUCTION

Most work on electron-spin-related research in GaAs has centered on *n*-type material because of the record spin lifetimes in excess of 100 ns [1]. In contrast, *p*-type GaAs has not been deemed a very promising material for electron-spin-related studies as electron spin relaxation via the Bir-Aranov-Pikus mechanism is generally extremely efficient in *p*-type systems [2]. More recent work, however, demonstrated that *p* doping with magnetic impurities such as Mn can lead to exceptionally long electron spin relaxation times in *p*-type GaAs [3]. This is due to antiferromagnetic exchange interaction between Mn ions and Mn acceptor bound holes, which results in a drastic suppression of the spin flip rates of electrons by the acceptors.

A prerequisite for optical studies of the spin dynamics of electrons in such a system is a detailed knowledge of the minority carrier lifetime. It is complicated by the fact that the latter is not constant, but sensitively depends on the exact experimental conditions and sample constituents. This can be understood by the very different rates of the possible decay channels. For example, the decay rate of an electron recombining with a hole in an exciton may exceed the rate of an electron recombining with a hole bound to an acceptor by as much as two orders of magnitude [4–6]. However, the former channel will not even be available for the minority carriers as long as there are no free holes in the valence band. Whether or not this is the case depends on the capture efficiency of free holes into acceptors and the number of available free acceptor states [7]. The latter number is completely sample dependent, while the former depends on the experimental parameters such as temperature and amount of optically created charge carrier pairs.

Consequently an optical determination of true carrier lifetimes in a specific sample requires knowledge about the decay of each electronic reservoir at the given experimental parameters. It is obviously impractical to measure each decay

for each needed parameter combination. In this paper, we show that it is possible to extract the full dynamics of the different carrier reservoirs by measuring the dependence of the exciton decay on excitation intensity by means of time-resolved photoluminescence (TRPL) spectroscopy. We invoke a numerical model based on Shockley-Read-Hall (SRH) recombination [8,9] that shows the crucial influence of the carrier population in shallow and deep recombination centers on the exciton lifetime. The model is applicable to any direct band-gap semiconductor that exhibits partial compensation.

## II. EXPERIMENT

Our measurements are performed on a 36  $\mu\text{m}$  thick GaAs:Mn layer grown by metal organic vapor phase epitaxy (MOVPE) on a (001) oriented GaAs substrate. The concentration of Mn acceptors is about  $N_{\text{Mn}} = 8 \times 10^{17} \text{cm}^{-3}$  and the sample exhibits partial compensation.

Photoexcitation is provided by an optical parametric amplifier [Light Conversion TOPAS-C, 110 fs, 785 nm (1.58 eV)] that is pumped by a regenerative amplifier system (Spectra Physics Spitfire Pro, 1 mJ, 1 kHz). The low duty ratio allows us to work with a fully relaxed system before each excitation pulse. The output is focused to a beam waist of about 350  $\mu\text{m}$ . The sample is mounted on the cold finger of an optical LHe cryostat ( $T = 8 \text{ K}$ ) with an angle of ca.  $60^\circ$  with respect to the direction of the incident laser beam and intersects the beam waist. The photoluminescence (PL) is collected at a  $90^\circ$  angle relative to the optical axis, passed through a 800 nm long-pass filter to separate the luminescence from the excitation and dispersed in a 300 mm focal length monochromator (Acton SP 2300i, equipped with a  $150 \text{ mm}^{-1}$  grating). The streak camera (Hamamatsu C 5680-22) is synchronized by a TTL signal from the regenerative amplifier. The observed time window can be shifted with a tunable, electrical delay line.

The low-energy tail of the excitation pulse is used to determine the time resolution of our setup. We find an instrumental response function (IRF), which can be accurately described by a Gaussian distribution with  $\sigma = 95 \text{ ps}$ .

---

<sup>\*</sup>tobias.kiessling@physik.uni-wuerzburg.de

<sup>†</sup><http://www.physik.uni-wuerzburg.de/EP3>

<sup>‡</sup><http://www.physik.uni-wuerzburg.de/EP6>

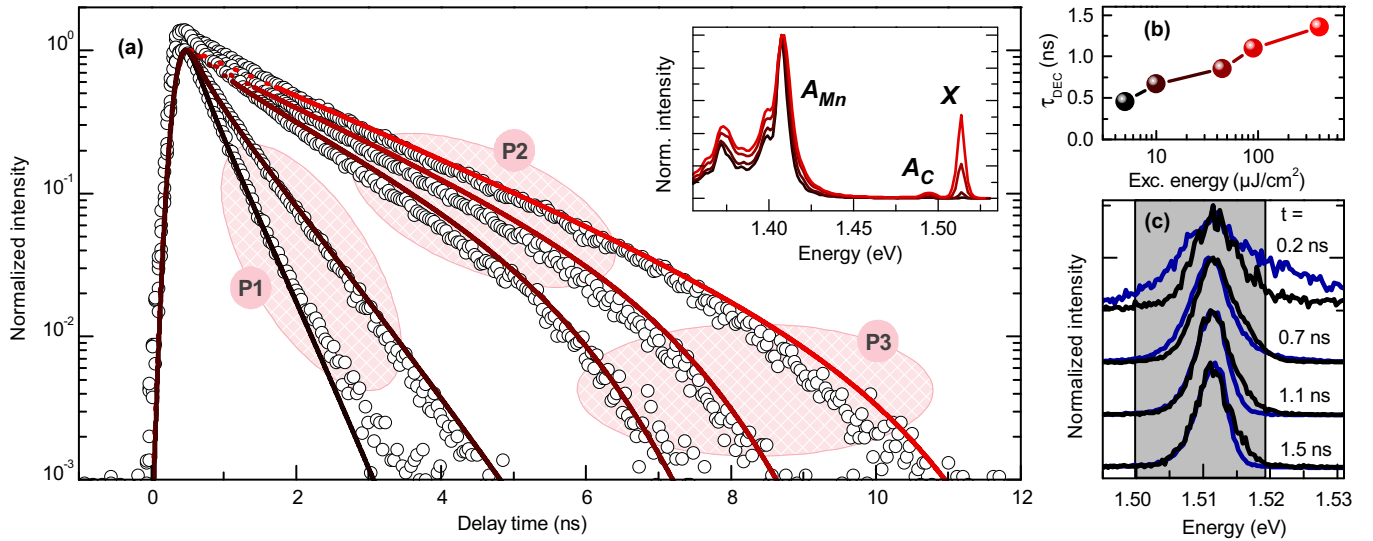


FIG. 1. (Color online) (a) Open circles: Exciton transients for different pulse energies [color encoding corresponds to plot (b)]. The modeled transients are plotted in solid lines. Inset: PL spectra at different cw-excitation power densities (taken from Ref. [3]), ranging from  $1 \text{ W cm}^{-2}$  (black) to  $50 \text{ W cm}^{-2}$  (red), normalized to the maximal intensity of the acceptor transitions. We identify excitonic ( $X$ ), shallow ( $A_C$ ) acceptor, and deep ( $A_{Mn}$ ) acceptor related transitions. (b) Decay times ( $1/e$ ) of exciton luminescence for different excitation pulse energies. (c) Excitonic spectra (black: lowest excitation power, blue: highest excitation power) at different delay times relative to the onset of luminescence. The gray shaded area indicates the spectral range, which is integrated to obtain the transients in (a).

Our numerical model has been implemented by the numerical integrator ODE45 from the MATLAB environment, which is based on the Runge-Kutta method for solving ordinary differential equations [10].

### III. RESULTS AND DISCUSSION

#### A. Data and analysis

Previous PL studies on the same sample under continuous wave (cw) excitation identified the relevant spectral features of the investigated material [see inset in Fig. 1(a)] [3]. A band of excitonic transitions is centered at  $1.51 \text{ eV}$ , which we ascribe to donor and acceptor bound excitons. Due to the high impurity concentration no individual transitions are resolved and the number of free excitons is negligible. The less pronounced peak at  $1.49 \text{ eV}$  is assigned to shallow carbon acceptors in GaAs [11]. The broad luminescence band around  $1.41 \text{ eV}$  stems from transitions involving Mn acceptor states [12]. A spectral resolution of the electron-acceptor ( $e, A^0$ ), donor-acceptor ( $D^0, A^0$ ) [13], or associated phonon lines [14] is again not possible. We observe a significant increase in spectral weight of the excitonic and the shallow acceptor transitions with increasing excitation power [3].

For the high pulse energies used in the current work (up to several hundreds  $\mu\text{J cm}^{-2}$ ), these transitions therefore dominate the TRPL signals, the result of which is summarized in Fig. 1(a). Since we cannot distinguish between different excitonic states, and the spectral shape of the excitonic luminescence is not shifting with time, we spectrally integrate the signal between  $1.502 \text{ eV}$  and  $1.519 \text{ eV}$  to establish time traces. The boundaries are chosen such that we limit the analysis to the exciton luminescence, distinguishing from ( $e, A^0$ ) transitions (lower boundary) and direct band-to-band (BB) transitions (upper boundary).

The data in Fig. 1 prove the concept of a universal, characterizing exciton lifetime to be strongly misleading. The decay rate depends not only on the excitation conditions but also on the elapsed time after the excitation pulse. We attribute this complex decay behavior to an intricate interplay between exciton and impurity states.

Specifically, it is driven by the varying effectiveness of available recombination channels for the excitons. Electron-hole pairs can recombine not only via direct radiative recombination of its constituents with each other, but can also lose their particles to ionized impurities. The decay rate of the latter recombination channel is mainly characterized by the number of available ionized impurities and their capture efficiency for electrons or holes.

We can loosely identify three distinguishing regimes in our data, designated with the labels P1, P2, and P3 in Fig. 1:

(i) P1: The decay times under weak excitation fall significantly below  $500 \text{ ps}$  (see also Fig. 4), which is clearly shorter than typical radiative decay times for free or bound excitons [4]. For low optical intensity in highly compensated material, trapping of photocarriers by ionized impurities is very effective due to the high number of available recombination centers, which gives rise to a very fast decay of exciton population.

(ii) P2: A pronounced prolongation of the exciton decay time  $\tau_{\text{DEC}}$  ( $1/e$ ) with increasing pump pulse energy is observed, which is the opposite of what pure semiconductor systems exhibit [4]. For increased optical intensities the available impurity sites will fill and eventually saturate. In this limit, the decay rate is given by the radiative exciton lifetime.

(iii) P3: For long delay at high optical intensity the exciton decay accelerates again. This suggests a further onset of recombination via impurities. We will show in the following that ( $e, A^0$ ) and ( $D^0, A^0$ ) transitions described in the SRH

picture create sufficient reionized trapping centers to accelerate the decay at long delay times.

The clear signature of this interplay in our data allows us to develop a model to probe impurity level dynamics only by observing exciton decay dynamics.

### B. Modeling

Before entering a quantitative model we utter the following considerations. Generally, decay may occur by Auger recombination, radiative recombination and recombination via impurities. The large spot size of the photoexcitation in combination with the small low-temperature carrier mobility in highly doped bulk GaAs allow us to neglect diffusive effects. The large thickness of the sample further justifies neglect of surface recombination at high pump levels. Because of the high binding energy of  $E_{Mn} = 110$  meV of the Mn acceptors, on which the electrons reside before excitation, impact ionization can safely be neglected at the chosen excitation energy. Finally, reemission of impurity trapped carriers to the band states is further deemed irrelevant at low temperatures.

For a quantitative description we build a model on the basis of the continuity equation for the carrier concentration in excited semiconductors [15]. The model does not incorporate the picosecond time scale high pump power effects such as electron-hole plasma [16,17] or Auger recombination [18]. However, this is no principal flaw for the description of the nonexponential decay and the increase in exciton lifetime, both of which are relevant at the ns scale [19]. Our model will therefore exhibit systematic deviations from the data of the exciton decay at fast time scales, but we emphasize that this is not crucial for the scope of the current work.

The remaining possible radiative processes in the illustrated spectral window in Fig. 1(c) are direct BB transitions as well as exciton recombination. Since we do not observe BB transition, we limit the model to excitonic transitions. As we can further not distinguish between different excitonic complexes, we take this radiative decay channel to be characterized by a radiative exciton lifetime  $\tau_{rr}$ .

The recombination via impurities in an excited semiconductor can be expressed with a rate equation in a Shockley-Read-Hall model. In the case of low temperature and/or compensated materials, the primordial rate expression reduces to

$$R_{SRH} = \left( \frac{\tau_{cap,p}}{p} + \frac{\tau_{cap,n}}{n} \right)^{-1} \quad (1)$$

with  $n, p$  being the extrinsically excited charge carriers and  $\tau_{cap,i}$  the capture time of electrons ( $n$ ) or holes ( $p$ ).

Here, the capture rate  $1/\tau_{cap,i}$  is proportional to the occupation of the corresponding impurity level:

$$\frac{1}{\tau_{cap,J,i}} = \sigma_{J,i} v_{th,i} N_J^{(0,\pm)} \quad (2)$$

with  $v_{th,i}$  being the thermal velocity of the charge carriers ( $i = n, p$  for electrons and holes, respectively),  $\sigma_{J,i}$  the capture cross section for a band carrier  $i$  by the impurity  $J$ , and  $N_J^{(0,\pm)}$  the concentration of trapping centers, which can be either neutral impurities (represented by the superscript 0) or positively charged donors (respectively, negatively charged acceptors) (represented by the corresponding sign).

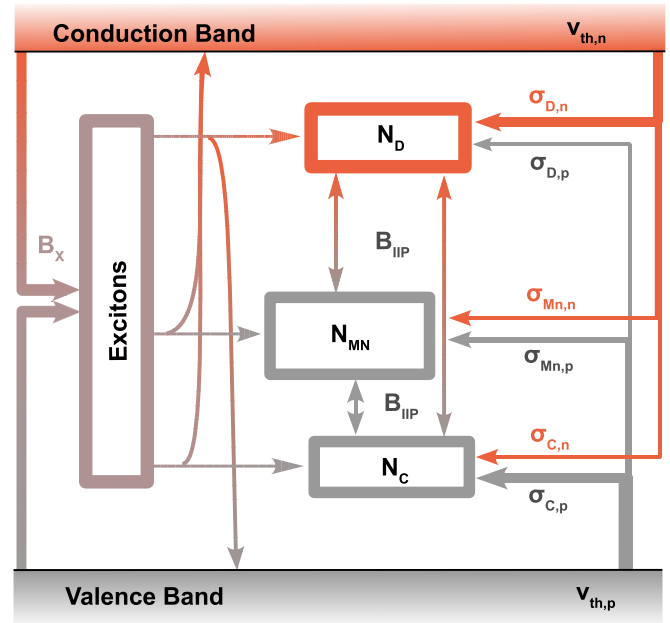


FIG. 2. (Color online) Schematic of the considered transitions between the electronic reservoirs after excitation: Photocarriers are created in the bands. They can leave the band by forming excitons or by impurity trapping. Trapping of constituents of excitons by the impurities releases the other particle as band charge carriers. The parameters defining the rates are indicated at each channel.

We assume impurity trapping of exciton bound charge carriers by the same mechanism, with the remaining charge carrier reemitted into the bands. This assumption is validated by the high impurity concentration in our sample. With the mean impurity spacing being smaller than typical exciton Bohr radii in GaAs [4], even bound excitons will find several impurity states to recombine with on average.

Finally, we consider interimpurity pair (IIP) recombination. This includes donor-acceptor pair recombination (DAP) as well as acceptor-acceptor pair relaxation (AAP), which enables the hole to relax into the energetically lower acceptor before recombination. An overview of the different reservoirs and the included relaxation channels is given in Fig. 2. (Initial carrier generation and radiative recombination of excitons are not shown for better clarity.)

We take the occupation of the reservoirs as the only time-dependent quantity, while all other parameters are supposed to be time independent.

We start the derivation of our model by listing the source and drain channels for the excitons. Considering radiative recombination and capture by impurities as drains, and taking the photogenerated band carriers as source (see left-hand side of Fig. 2), the dynamics in the exciton population are described by

$$\frac{dn_X}{dt} = G_X - \frac{n_X}{\tau_{rr}} - \sum_{J,i} \frac{n_X}{\tau_{cap,J,i}}, \quad (3)$$

where  $n_X$  is the number of excitons and  $G_X$  defines their generation rate.

From Eq. (2), the value of  $\tau_{cap}$  depends on the occupation  $N_J^{\pm}$  of the ionized impurity levels. It is therefore evident that

the exciton decay  $dn_X/dt$  and impurity state dynamics are directly coupled.

Following this argumentation, a solution of Eq. (3) cannot be achieved without the simultaneous solution of the equations for each impurity level  $dN_J^\pm/dt$ . Their capture and relaxation

channels are depicted on the right-hand side of Fig. 2. Our model hence encompasses six coupled rate equations on the population of the six considered electronic reservoirs, given explicitly by

$$\begin{aligned}
 \frac{dn}{dt} &= G & -npB_X & & +n_X/\tau_{\text{cap},Mn,p} + n_X/\tau_{\text{cap},C,p} & -n/\tau_{\text{cap},D,n} & -n/\tau_{\text{cap},Mn,n} & -n/\tau_{\text{cap},C,n} \\
 \frac{dn_X}{dt} &= & npB_X & & -n_X/\tau_{rr} & -n_X/\tau_{\text{cap},D,n} & -n_X/\tau_{\text{cap},Mn,p} & -n_X/\tau_{\text{cap},C,p} \\
 \frac{dN_D^+}{dt} &= & -n/\tau_{\text{cap},D,n} + p/\tau_{\text{cap},D,p} & & -n_X/\tau_{\text{cap},D,n} & & +B_{IIIP}N_D^0N_{Mn}^0 & +B_{IIIP}N_D^0N_C^0 \\
 \frac{dN_{Mn}^-}{dt} &= & -p/\tau_{\text{cap},Mn,p} + n/\tau_{\text{cap},Mn,n} & & -n_X/\tau_{\text{cap},Mn,p} & & +B_{IIIP}N_D^0N_{Mn}^0 & -B_{IIIP}N_{Mn}^-N_C^0 \\
 \frac{dN_C^-}{dt} &= & -p/\tau_{\text{cap},C,p} + n/\tau_{\text{cap},C,n} & & -n_X/\tau_{\text{cap},C,p} & & +B_{IIIP}N_D^0N_C^0 & +B_{IIIP}N_{Mn}^-N_C^0 \\
 \frac{dp}{dt} &= G & -npB_X & & +n_X/\tau_{\text{cap},D,n} & -p/\tau_{\text{cap},D,p} & -p/\tau_{\text{cap},Mn,p} & -p/\tau_{\text{cap},C,p}
 \end{aligned} \tag{4}$$

The generation term  $G$  is taken to be a Gaussian in time, normalized to the total number of electrons (holes) created by a single light pulse. For our experimental conditions all photocarriers are considered to be excited as uncorrelated band carriers. We thus introduce a parameter  $B_X$  that describes exciton formation from band carriers. The density of a particular ionized (neutral) impurity is indicated by  $N_J^\pm$  ( $N_J^0$ ) with  $N_J^0 = N_{J,\text{tot}} - N_J^\pm$ , with the indices  $D$ ,  $C$ , and  $Mn$  accounting for shallow donors, carbon acceptors and manganese acceptors, respectively. Most of the model parameters are known in the literature and summarized in Table I.

We determine the density of photocreated charge carriers in  $G$  by measuring the pulse energy in front of our cryostat, accounting for reflection losses at the window of the cryostat and the sample surface [23]. The penetration depth of the excitation wavelength is in the order of  $1 \mu\text{m}$  [24], resulting in  $2.5 \times 10^{16} \text{ cm}^{-3}$  to  $2 \times 10^{18} \text{ cm}^{-3}$  photocarrier pairs per pulse for the given experimental conditions. As the model is incapable of incorporating  $e$ - $h$  plasma recombination, we have to estimate the initial loss by this channel and correct for it. Taking the spectral weight of the spectrally broadened luminescence profile at short delays [see Fig. 1(c)], we estimate an upper limit of 15%, which is the value used for the remainder of this work.

Due to the small emission probability of optical phonons at low temperatures, it is well established that photocarriers are

TABLE I. Overview of coefficients used in the model with reference if applicable.

Parameter	Value	Unit	Reference
$B_X$	$1 \times 10^6$	$\text{cm}^3 \text{ s}^{-1}$	
$B_{IIIP}$	$1 \times 10^{-11}$	$\text{cm}^3 \text{ s}^{-1}$	[20]
$\sigma_{D,n}$	$5 \times 10^{-15}$	$\text{cm}^2$	[5]
$\sigma_{D,p}$	$1 \times 10^{-16}$	$\text{cm}^2$	[21]
$\sigma_{Mn,n}$	$2 \times 10^{-18}$	$\text{cm}^2$	[14]
$\sigma_{Mn,p}$	$2 \times 10^{-15}$	$\text{cm}^2$	[14]
$\sigma_{C,n}$	$1 \times 10^{-16}$	$\text{cm}^2$	[5]
$\sigma_{C,p}$	$8 \times 10^{-14}$	$\text{cm}^2$	[5]
$\tau_{rr}$	$2 \times 10^{-9}$	s	[22]
$T_{cc}$	20	K	

not in thermal equilibrium with the lattice for our experimental conditions [25]. In accordance with recent studies, which show the temperature may exceed the lattice temperature clearly in case of pulsed excitation [16,26], the average charge carrier temperature is set to 20 K. This results in a thermal velocity of  $12 \times 10^6 \text{ cm s}^{-1}$  for electrons resp.  $5 \times 10^6 \text{ cm s}^{-1}$  for holes [27].

The recombination rate via interimpurity pair recombination is chosen such that the model properly describes the observed slow decay of the  $(D^0, A_{Mn}^0)$  transitions (not shown). By this we obtain DAP lifetimes in quantitative good agreement with earlier work, i.e.,  $\tau_{\text{DAP}} \approx 100 \text{ ns}$  for an excitation energy of  $1 \mu\text{J cm}^{-2}$  [20].

The onset of the luminescence provides an upper limit for the formation coefficient of excitons  $B_X$  in our sample. A higher value for  $B_X$  would shift the maximum of the luminescence to larger delay times and thus contradict our data. Since a detailed study of exciton formation dynamics is not central to this paper, we confine ourselves with this estimate assuring exciton formation in a few picoseconds, which can be found as a usual value in literature [16,28]. The exciton radiative recombination time  $\tau_{rr} = 2 \text{ ns}$  is taken to be an average of usual exciton lifetimes in GaAs [22].

The values for  $\sigma_{J,n}$  as well as the hole capture cross section  $\sigma_{C,p}$  of the carbon acceptor are well known in the literature [5,14].

Although we cannot observe the donor-hole transition directly, we include it for symmetry reasons [29]. Explicit values for the hole capture cross section of shallow donors are, however, not available. A study on deeper impurities finds hole capture cross sections for a variety of donors [21] not exceeding  $1 \times 10^{-16} \text{ cm}^2$ . Bearing in mind that donor-hole transitions are not the leading order in our case, we use this limit for our model.

Hole capture cross sections for the deep Mn acceptor are only available from deep level transient spectroscopy (DLTS) [14] and have to be treated with caution, as there are indications that these are unsuitable for PL analysis [30]. We were unable to obtain appreciable agreement of model and data, unless assuming slightly smaller values for  $\sigma_{Mn,p}$  in our model than given by Ref. [14].

The initial values for  $n$ ,  $p$ , and  $n_X$  are set to zero, motivated by Mn being the dominating impurity, its high ionization

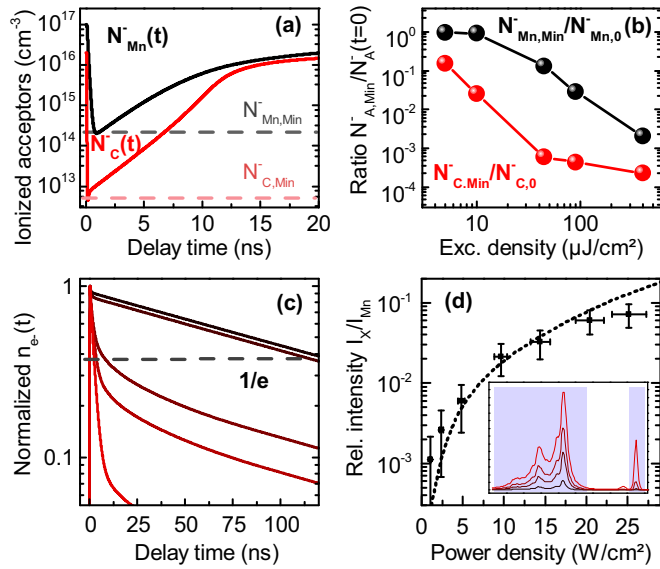


FIG. 3. (Color online) Model repercussions: (a) Modeled transients of  $N_{\text{Mn}}^-$  ( $N_{\text{C}}^-$ ) at highest excitation power density. (b) Ratio of minimal number of  $N_{\text{A}}^-$  after excitation [indicated in (a)] and the initial value of  $N_{\text{A}}^- (t=0)$ . (c) Accumulated electron population after the excitation (see text). Color scheme is chosen according to Fig. 1(b). Measured intensity ratios of the optical transitions (crosses) for cw excitation compared to the prediction made by the model. The inset shows the spectral regimes which were integrated.

energy, and the low temperature. From this it follows that the total donor and carbon acceptor concentration equal their initial ionized concentrations, whereas the Mn acceptor is only partially ionized.

The starting conditions for the impurity reservoir are an initially ionized donor concentration of  $4 \times 10^{16} \text{ cm}^{-3}$ , an ionized carbon acceptor concentration  $2 \times 10^{16} \text{ cm}^{-3}$ , and an ionized Mn acceptor concentration of  $10 \times 10^{16} \text{ cm}^{-3}$  (see Sec. A for further discussion). Using these values in combination with the parameter given in Table I, we are able to describe the data with our model to good accuracy [see Fig. 1(a)]. As a general remark, we note that despite the obvious uncertainties in the model parameters, only a very small interval of allowed values produces satisfactory agreement between model and data.

### C. Discussion

Solving Eqs. (4) we are able to extract the temporal evolution of the occupation in each reservoir. We show two representative time traces  $N_{\text{Mn}}^- (t)$  and  $N_{\text{C}}^- (t)$ , modeled with the highest excitation power density [see Fig. 3(a)]. We note the rapid hole capture of the ionized impurities, reducing the number of available ionized impurities. This process takes place directly after the excitation. After reaching its minimal degree of ionization, the acceptors reionize due to  $(e, A^0)$  and  $(D^0, A^0)$  recombination and AAP relaxation. The time traces of the reservoirs for other excitation energies look qualitatively similar, but differ strongly in the obtained minimal degree of ionization after the excitation, as shown in Fig. 3(b). The observed features of the exciton decay are readily understood from these plots.

TABLE II. Recombination channel decay rates.

Channel	P1	P2	P3
Rad. rec.	1/(2 ns)	1/(2 ns)	1/(2 ns)
$N_{\text{C}}^-$ trapping	1/(800 ps)	1/(32 ns)	1/(1.74 ns)
$N_{\text{Mn}}^-$ trapping	1/(1.1 ns)	1/(93 ns)	1/(18 ns)
Total	1/(444 ps)	1/(1.86 ns)	1/(820 ps)
Expt.	1/(400 ps)	1/(1.45 ns)	1/(850 ps)

P1. From Fig. 3(b) we extract that in this regime the number of ionized impurities is hardly affected by the photocarriers. We therefore have a large reservoir of trapping centers available at all times, which leads to a rapid decay of the exciton population.

P2. Figures 3(a) and 3(b) demonstrate the dramatic decrease in the number of ionized impurities at high excitation energies. At 5 ns the total number is still orders of magnitude lower than in the low-excitation case. The recombination via impurity trapping is hence negligible, and the decay can be described by the radiative exciton lifetime.

P3. At 10 ns the system has already partially recovered from the excitation, and the amount of ionized impurities has increased by a factor of 5–20 compared to 5 ns. Consequently impurity trapping again starts to contribute sizeably, and the overall decay accelerates.

It is further instructive to directly look at the decay rates of the different channels in the respective time regimes, which we provide below in Table II.

In many experiments, e.g., spin lifetime studies, one will mainly be concerned with the time evolution of the total number of electrons (i.e., the minority carriers) in the system. The overall electron population  $n_{e^-}$  can easily be extracted from the solution of the equation system. Photoexcited electrons end up either as free carriers in the conduction band  $n(t)$ , as exciton constituents  $n_X(t)$  or on neutralized donors  $N_{D,\text{tot}} - N_D^+(t)$ . Thus we can obtain the total number of electrons in the system at any time after the excitation by adding the occupation of these reservoirs, as summarized in Fig. 3(c). A massive decrease in the  $1/e$  lifetime of the electrons is observed with increasing pump power, which stems from the availability of the fast radiative exciton decay channel at these conditions. While carrier capture onto impurity states is rapid, the impurity electron-hole recombination is not.

We substantiate our conclusion by two further considerations. First, we are also in a position to discuss the cw data from our results. In this situation, the generation term in Eqs. (4) has to be modified to a constant value according to the applied excitation power, and the thermal velocity has to be adapted to the excitation conditions [31]. After 5000 ns the system reaches a balanced state, which is comparable to the cw case. From this, we can deduce the relative intensities of the optical transitions by extracting the radiative decay channels from the equations.

We find a good quantitative agreement between data and model over the observed power range [see Fig. 3(d)] for the comparison between the intensities of the exciton transitions and the Mn-acceptor-related transitions.

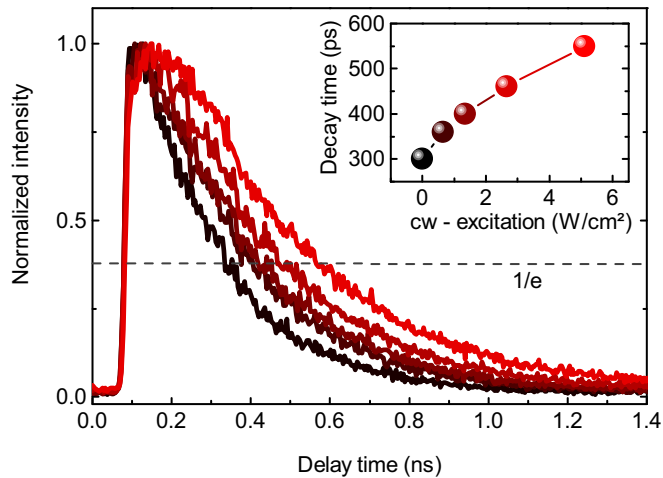


FIG. 4. (Color online) Influence of additional cw excitation on the exciton lifetime. The fluence was less than  $1 \mu\text{J cm}^{-2}$ . The inset shows the increase of the decay time ( $1/e$ ). The color encodings correspond to each other.

Second, we can corroborate the interplay between exciton decay time and the concentration of ionized impurities by changing the amount of ionized impurities. We therefore perform a test experiment with additional cw illumination and measure again TRPL at constant pulsed excitation energy density. We choose a lower excitation energy compared to the data in Fig. 1 to demonstrate the effect for common cw excitation conditions. Therefore we use a different pulsed light source (Spectra Physics, 100 fs, 795 nm) as well as a further cw Laser (Coherent Cube, 785 nm). The result is shown in Fig. 4. We can clearly control the exciton decay time by only tuning the intensity of the cw source, consistent with our model predictions.

#### IV. CONCLUSION

To conclude, we observed a pronounced dependence of the exciton decay in partially compensated *p*-type GaAs on the excitation conditions. The invoked model enables us to trace this on the impact of impurity capture on the exciton decay and allows us extract the occupation dynamics of the impurity

system. The agreement between data and model for both the cw and pulsed excitation, demonstrates the reliability of the model over a broad range of experimental parameters.

#### ACKNOWLEDGMENTS

The authors gratefully acknowledge support by the DFG (Projects No. INST 93/623-1 FUGG and No. OS98/9-3).

#### APPENDIX

In the following, we discuss the uncertainties of the values entering our model that cannot be found in the literature and their respective impact on the overall model results.

*Impurity concentrations.* The sample is characterized by standard Hall measurements, which reveal a Mn acceptor concentration of  $8 \times 10^{17} \text{ cm}^{-3}$  and a shallow impurity imbalance ( $\Delta N = N_D - N_C$ ) of  $2 \times 10^{16} \text{ cm}^{-3}$ . We know from cw data that the carbon acceptor concentration is significantly smaller than the manganese concentration. We therefore assume the concentration of shallow impurities to be itself of the order of magnitude of the impurity imbalance.

We find the best agreement of model and data for the values  $N_D = 4 \times 10^{16} \text{ cm}^{-3}$  and  $N_A = 2 \times 10^{16} \text{ cm}^{-3}$ . The best fitting value of  $N_{\text{Mn}}^-(t=0) = 10 \times 10^{16} \text{ cm}^{-3}$  corresponds to approximately 10% of the whole Mn concentration. We believe the discrepancy of  $N_{\text{Mn}}^-$  and  $N_D - N_C$  is well explained by Mn atoms situated on interstitial sites acting as double donors [32].

*Mn capture cross section.* The last parameter to be discussed is the manganese hole capture cross section  $\sigma_{\text{Mn},p}$ . To our knowledge, the only cross-section studies on the Mn acceptor in GaAs have been performed by Montelius *et al.* [14]. The authors used deep-level transient spectroscopy (DLTS) for determining the hole capture cross section  $\sigma_{\text{Mn},p}$  and TRPL to study the electron capture cross section  $\sigma_{\text{Mn},n}$ . Whereas the published value for  $\sigma_{\text{Mn},n}$  fits very well to our data, the value of  $\sigma_{\text{Mn},p}$  deviates nearly for an order of magnitude in our model. A value in accordance to DLTS data would drastically accelerate the decay for all observed injection levels. Since the authors have later pointed out that it might be inappropriate to use cross-section values from DLTS in other situations [30], we attribute the observed deviations to this consideration. The value itself can again be varied only in a small interval (to within a factor of 2) within the model without producing significant deviations from the data.

- 
- [1] R. I. Dzhioev, K. V. Kavokin, V. L. Korenev, M. V. Lazarev, B. Ya. Meltser, M. N. Stepanova, B. P. Zakharchenya, D. Gammon, and D. S. Katzer, *Phys. Rev. B* **66**, 245204 (2002).
  - [2] G. L. Bir, A. G. Aronov, and G. E. Pikus, *Zh. Eksp. Teor. Fiz.* **69**, 1382 (1975) [*Sov. Phys. JETP* **42**, 705 (1976)].
  - [3] G. V. Astakhov, R. I. Dzhioev, K. V. Kavokin, V. L. Korenev, M. V. Lazarev, M. N. Tkachuk, Yu. G. Kusrayev, T. Kiessling, W. Ossau, and L. W. Molenkamp, *Phys. Rev. Lett.* **101**, 076602 (2008).
  - [4] G. W. p't Hooft, W. A. J. A. van der Poel, L. W. Molenkamp, and C. T. Foxon, *Phys. Rev. B* **35**, 8281(R) (1987).
  - [5] D. Bimberg, H. Münzel, A. Steckenborn, and J. Christen, *Phys. Rev. B* **31**, 7788 (1985).
  - [6] I. A. Akimov, R. I. Dzhioev, V. L. Korenev, Yu. G. Kusrayev, E. A. Zhukov, D. R. Yakovlev, and M. Bayer, *Phys. Rev. B* **80**, 081203(R) (2009).
  - [7] A. Lohner, M. Woerner, T. Elsaesser, and W. Kaiser, *Phys. Rev. Lett.* **68**, 3920 (1992).
  - [8] W. Shockley and W. T. Read, *Phys. Rev.* **87**, 835 (1952).
  - [9] J. S. Blackmore, *Semiconductor Statistics*, Vol. 3. (Pergamon Press, Oxford, 1962).
  - [10] J. R. Dormand and P. J. Prince, *J. Comp. App. Math.* **6**, 19 (1980).

- [11] D. J. Ashen, P. J. Dean, D. T. J. Hurle, J. B. Mullin, A. M. White, and P. D. Greene, *J. Phys. Chem. Solids* **36**, 1041 (1975).
- [12] T. C. Lee and W. W. Anderson, *Solid State Commun.* **2**, 265 (1964).
- [13] W. Schairer and M. Schmidt, *Phys. Rev. B* **10**, 2501 (1974).
- [14] L. Montelius, S. Nilsson, L. Samuelson, E. Janzen, and M. Ahlström, *J. Appl. Phys.* **64**, 1564 (1988).
- [15] S. M. Sze and K. K. Ng, *Physics of Semiconductor Devices* 3rd ed. (Wiley, New York, 2007).
- [16] A. Amo, M. D. Martín, L. Vina, A. I. Toropov, and K. S. Zhuravlev, *Phys. Rev. B* **73**, 035205 (2006).
- [17] S. Tanaka, H. Kobayashi, H. Saito, and S. Shionoya, *Solid State Commun.* **33**, 167 (1980).
- [18] U. Strauss, W. W. Rühle, and K. Köhler, *Appl. Phys. Lett.* **62**, 55 (1993).
- [19] It is technically not a problem to incorporate Auger terms, but they will not bear any physical meaning as long as they are not distinguishable from Coulomb effects, which in our data they are not.
- [20] I. A. Akimov, R. I. Dzhoiev, V. L. Korenev, Yu. G. Kusrayev, V. F. Sapega, D. R. Yakovlev, and M. Bayer, *J. Appl. Phys.* **113**, 136501 (2013).
- [21] A. Mitonneau, A. Mircea, G. M. Martin, and D. Pons, *Rev. Phys. Appl.* **14**, 853 (1979).
- [22] C. J. Hwang, *Phys. Rev. B* **8**, 646 (1973).
- [23] Sadao Adachi, *Phys. Rev. B* **41**, 1003 (1990).
- [24] M. D. Sturge, *Phys. Rev.* **127**, 768 (1962).
- [25] H. Münzel, A. Steckenborn, and D. Bimberg, *J. Lumin.* **24-25**, Part 2(0), 569 (1981).
- [26] T. Henn, T. Kiessling, W. Ossau, L. W. Molenkamp, D. Reuter, and A. D. Wieck, *Phys. Rev. B* **88**, 195202 (2013).
- [27] For sake of simplicity we take the temperature to be constant over the observed time window. We emphasize that the effect of an accelerated decay at long delay times cannot be associated with a temperature decrease. A pronounced carrier cooling would instead result in a decrease of the exciton decay rate due to reduced thermal velocities, opposite to what is observed.
- [28] Rajesh Kumar, A. S. Vengurlekar, S. S. Prabhu, Silvano De Franceschi, and Fabio Beltram, *Phys. Rev. B* **54**, 17591 (1996).
- [29] R. Ulbrich and B. Moreth, *Solid State Commun.* **14**, 331 (1974).
- [30] L. Montelius, S. Nilsson, and L. Samuelson, *Phys. Rev. B* **40**, 5598 (1989).
- [31] T. Kiessling, J.-H. Quast, A. Kreisel, T. Henn, W. Ossau, and L. W. Molenkamp, *Phys. Rev. B* **86**, 161201(R) (2012).
- [32] Steven C. Erwin and A. G. Petukhov, *Phys. Rev. Lett.* **89**, 227201 (2002).